Prescission charged particle emission in $^{19}F+^{232}Th$

A. Chatterjee, A. Navin, S. Kailas, P. Singh, D.C. Biswas, A. Karnik, and S.S. Kapoor
Nuclear Physics Division, Bhabha Atomic Research Centre, Bombay 400 085, India
(Received 2 June 1995)

The multiplicities of prescission protons and α particles in the reaction $^{19}F+^{232}Th$ at 104, 110, 116, and 118 MeV have been measured. The observed multiplicities are much larger than the prediction of the statistical model without the introduction of fission delay. An analysis of the prescission proton and α data along with that for neutrons (measured earlier) has been made using deformed optical model and deformation-dependent particle binding energies. Simultaneous fits to the charged particle and neutron data required a total fission time scale in the range of $(25-80)\times 10^{-21}$ s. For this system, the mean kinetic energies of the prescission particles are insensitive to the division of the total delay time into presaddle and postsaddle components; however, the neutron and charged particle multiplicity data are sensitive to the deformation of the saddle-to-scission emitter. The analysis shows that postsaddle emission takes place close to the scission point.

PACS number(s): 25.70.Jj, 25.85.Ge

I. INTRODUCTION

From studies of heavy-ion-induced fission, it is well established that the influence of nuclear friction leads to the dramatic effect of a time delay of 10–50 zs (1 zs = 10^{-21} s) in the fission process. Time scales in heavy-ion-induced fission have been deduced from the multiplicities of prescission neutrons, ν_{pre} [1–4], protons, and α particles, π_{pre} and α_{pre} [5–8], and electric dipole γ rays, γ_{pre} [9]. Analysis of ν_{pre} data leads to the conclusion that the time of fission, t_{fiss}, is much longer than that predicted by the standard statistical model (without friction), implying that dynamics of the fission process involves overdamped motion. This is supported by transport models which describe the time evolution of the fission process, taking into account the dissipative effect of friction [10].

Prescission neutron multiplicities can be calculated using the statistical model. The excess of the experimentally observed ν_{pre} values over the calculated ones serves as a "neutron clock" to estimate the fission time delay. In this manner, the fission time scales have been extracted for a number of systems. In the "neutron clock thermometer" method [3], the measured mean neutron kinetic energy is used as an additional constraint to fix t_{fiss} and the average excitation energy of the emitting systems, thereby establishing that, in heavy systems, the emission of neutrons takes place mainly from the large deformations near scission, implying that dissipation is stronger nearer the scission point. However, it is rather difficult to separate the total fission time scale t_{fiss} into presaddle (t_d) and saddle-to-scission (t_{ssc}) components. The observed delay also contains a component t_{fo} arising from the formation phase of the compound nucleus. In an earlier work [4], by considering the ν_{pre} data for a large number of systems and its entrance channel dependence, the systematics of the individual time scales t_{fo}, t_d, and t_{ssc} were obtained.

The measurement of prescission proton and α particle multiplicities (π_{pre} and α_{pre}) provides another clock for the measurement of fission time scales [5,6]. The interpretation of these data requires consideration of the fact that charged particle emission depends upon the Coulomb barrier of the exit channel which is sensitive to the deformation of the emitter. In the analysis [5] of the data for ^{200}Pb, ^{213}Fr, ^{216}Ra, ^{225}Np, and ^{236}Cm compound nuclei, the lowering of the emission barriers by $\sim$1.2 MeV for protons and $\sim$2.0 MeV for alphas was found to be sufficient to account for the measured multiplicities and no fission delay was required. It was, however, later shown [7] that the suppression of charged particle emission (for systems with $A\sim 200$) could result due to the expected increase of particle binding energies B_{part} with deformation, and when this was taken into consideration, the charged particle data also required a fission delay, and thus, it was possible to explain the charged particle and neutron data in a consistent manner. In Ref. [7] by considering the experimental values of the mean emission kinetic energies in addition to the multiplicities of the prescission particles, the time scales t_d, t_{ssc} and the average deformation of the saddle to scission emitter, Z_{axis}, could be determined. On the basis of the systematics presented earlier [4], it is expected that t_d is constant and about 10 zs for a large range of fissility (χ) values, whereas t_{ssc} shows a linear variation from about 3 zs to 50 zs for χ in the range of 0.70–0.85. The increase in t_{ssc} with χ can be qualitatively understood [3] in terms of the potential energy surface, there being a longer deformation path to be covered in the passage from saddle-to-scission for larger χ.

The crucial questions connected with the emission of particles during the evolution of the fissioning system are the time scales and deformations involved. In order to explore these aspects it is necessary to consider systems spanning a wide range of fissilities. The recent measurement [8] of $^{19}F+^{159}Tb$ is useful for the low fissility domain (however, the analysis in [8] does not include the effect of deformation on B_{part}). In the present work we have measured π_{pre} and α_{pre} for $^{19}F+^{232}Th$ at beam energies of 104, 110, 116, and 118 MeV in order to obtain fission lifetime information for a system with large fissility. Neutron multiplicities for this system are available from an earlier measurement [2].

The data have been analyzed using the statistical model code JOANNE2 [7] with deformed optical model calculations

of the particle transmission coefficients T_l and deformed liquid drop model for B_{part}. The parameters t_d, t_{ssc}, and Z_{axis} were varied to simultaneously fit the charged particle and neutron data. Here the deformation Z_{axis} is defined as the elongation of the emitter in units of the diameter of the spherical system. The average kinetic energies of the prescission particles are found to be insensitive to the individual delays t_d and t_{ssc}. However, the multiplicity data are sensitive to Z_{axis}.

II. EXPERIMENTAL METHOD

The measurements were made with ^{19}F beams at the BARC-TIFR 14UD Pelletron facility in the general purpose 1 m diameter scattering chamber. The targets were self-supporting rolled foils of ^{232}Th, $\sim$2 mg/cm^2 thick.

The fission fragment detector was a trapezoidal position-sensitive gridded ionization chamber telescope consisting of ΔE_{gas} and E_{gas} elements. The anode corresponding to the ΔE signal was segmented so as to obtain position information by the pulse division method. The fission fragments were clearly separated from beamlike particles in the ΔE-E plot. The detector covered an angular range of 30° and a solid angle of 70 msr. Further details about the fission detector are given elsewhere [11].

Protons and α particles were detected in two NaI detectors with Havar foil windows, designed for the detection of charged particles in vacuum. These detectors were 45 mm diameter and were placed at distances $\sim$112 mm from the target position resulting in an angular spread of $\sim$22° and solid angles $\sim$115 msr. Large solid angles were selected in view of the low coincidence rates, although at the cost of angular resolution. The detectors were covered by 40 mg/cm^2 thick Ta foils to stop beamlike particles. Separation of particles was achieved by pulse shape discrimination, exploiting the rise time differences of the detector response to different radiations [12]. Protons, deuterons, tritons, α particles, and γ rays were well separated in the two-dimensional plot of pulse shape against pulse height except at the lowest energies. Because of the difficulty with pulse-shape discrimination at lower energies, and because foil covers were used, only the measured spectra above 2 MeV protons and 12 MeV α particles have been considered in the analysis.

In order to eliminate possible contamination of the measured spectra because of the sensitivity of the detectors to neutrons, a separate measurement was made covering one of the NaI detectors by a 1 mm thick Ta foil. Singles spectra were recorded in the two detectors placed at $\pm$40° to the beam. A comparison of the spectra showed that the contribution of neutrons to the measured prefission charged particle spectra was negligible in the energy range considered.

The NaI detectors were calibrated for α particles with a ^{229}Th source after removing the Ta foil covers making use of the five α energies 6.288, 6.778, 7.067, 8.377, and 8.785 MeV. On taking account of the energy loss in the Havar foil, a linear calibration curve could be obtained and this was used to calibrate the measured spectra correcting for the energy losses in the Havar and Ta foils. The calibration for protons was done in beam, with a Mylar target, detecting recoil protons from the elastic and inelastic scattering of ^{19}F from ^{1}H. In order to reduce the kinematic broadening, the NaI detector was kept at 0°, the ^{19}F beam being stopped on a 40 mg/cm^2 Ta backing behind the Mylar target. Beam energies in the range of 78–116 MeV were used. The proton spectra showed the elastic recoil peak and the inelastic peak from the projectile excitation to 1.346 MeV. The maximum error in calibrated energies in the range of the measured spectra is 0.5 MeV, arising in the case of α particles from the extrapolation of the calibration curve and, in both cases, from the corrections required for the Ta foils.

In order to test the accuracy of the energy calibration of the NaI detectors, a surface-barrier ΔE-E telescope was also used in the experiments. Although the solid angle, 33 msr, was too low to be of value for coincidence data, a comparison of singles spectra at overlapping angles was done. This was useful since the telescope calibration did not have to be corrected for foil covers. The surface barrier telescope was also used to check the solid angles of the NaI detectors which were more difficult to determine directly from the geometry because of the close distance from the target.

In the experimental geometry, the NaI detectors were placed at 40° central angle on either side of the beam direction, while the fission detector was placed to cover the angular range from 115° to 145°. The coincidence charged particle spectra include contributions from the emission from the compound nucleus (CN) and each of the fission fragments (FF's). The procedure to separate the spectra into pre- and postscission contributions relies upon the Coulomb barrier difference for the two emitting systems (CN and FF) and kinematic focusing effects. Post scission particles are emitted isotropically in the rest frame of the fission fragments and in the laboratory frame are focused in the direction of emission of the fragments. The focusing effect is stronger for α particles than for protons. The geometry was chosen to maximize the difference in kinematical effects for the two charged particle detectors, one covering angles around 90° to the detected fragment, the other covering angles around 0° to the complementary fragment. Data were also taken in another geometry, with the fission detector centered around +135° and the charged particle detectors at −30° and −110°.

The data were recorded in the multiparameter list mode, the event trigger condition being generated from the coincidence of the fission detector with either of the NaI detectors. The TAC outputs of the two NaI detectors with respect to the fission detector were recorded and used to correct for chance coincidences. The singles fission events from the ionization chamber were prescaled by a factor of 15 and mixed into the event trigger. Thus both coincidence and singles data were recorded simultaneously, and the charged particle multiplicities could be extracted from the ratio of coincidence to singles counts.

The data reduction was carried out off line. Fission-proton and fission-α particle coincidence spectra were generated by imposing three separate gate conditions on the fission detector position each with an angular spread of 10° with appropriate banana gates to select fission events in the ionization chamber and protons or α particles in each of the NaI detectors.

III. ANALYSIS OF SPECTRA

The multiplicities for pre- and postscission charged particle emission were obtained by fitting the measured coinci-

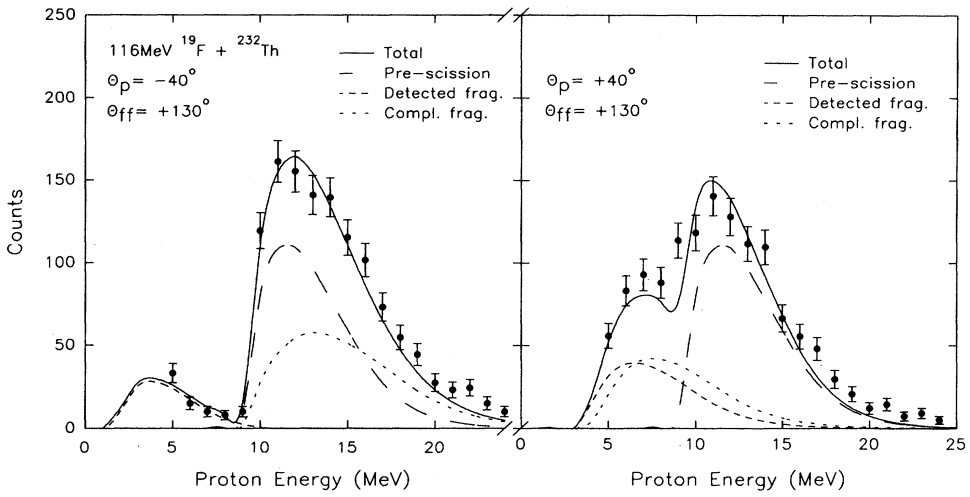

FIG. 1. Measured coincidence proton spectra, and fits showing the contributions of prescission emission, and emission from the two fragments. For the sake of clarity, overlapping curves have been displaced slightly.

dence spectra with a calculation assuming emission from the compound nucleus and from the detected and complementary fragments. For α emission there is also a near-scission emission (NSE) component [13]; however, this has not been included in the analysis, as NSE multiplicities are likely to be small [7].

The analysis of the spectra requires consideration of the large acceptance angles of both charged particle and fission detectors. This was done by writing a computer program in which center-of-mass emission spectra were calculated and transformed to appropriate laboratory angles. The laboratory spectra were integrated over the acceptance angles of the charged particle detectors and, in the case of postscission emission, also averaged over the bin of acceptance angles of the position sensitive fission detector.

The center-of-mass spectra for pre- and postscission emission were calculated using a constant-temperature level density formula, expressing the pre- and postscission components as

$$n_{\rm pre}(\epsilon)=\mu_{\rm pre}\epsilon\sigma_{\rm CN}(\epsilon)\exp(-\epsilon/T_{\rm CN}), \quad (1)$$

$$n_{\rm post}(\epsilon)=\mu_{\rm post}\epsilon\sigma_{\rm FF}(\epsilon)\exp(-\epsilon/T_{\rm FF}), \quad (2)$$

where $\mu_{\rm pre}$ and $\mu_{\rm post}$ are the pre- and postscission multiplicities ($=\pi_{\rm pre}$ and $\alpha_{\rm pre}$ for proton and alpha emission, respectively), $\sigma_{\rm CN}(\epsilon)$ and $\sigma_{\rm FF}(\epsilon)$ are the optical reaction cross sections for the emission from compound and fragment nuclei, and $T_{\rm CN}$ and $T_{\rm FF}$ are the appropriate temperatures. The temperatures have not been varied in the fits and were fixed from the estimated excitation energies and taking level density parameters of $a=A/10$ MeV^{-1} and $A/8$ MeV^{-1} for CN and FF, respectively. The excitation energy of fission fragments was estimated assuming symmetric division, taking fragment kinetic energies from systematics [14] and correcting for prescission neutrons using the measured [2] prescission neutron multiplicities. The temperatures $T_{\rm CN}$ and $T_{\rm FF}$ were about 1.52 and 1.63 MeV, respectively, varying slightly with beam energy.

The optical reaction cross sections $\sigma_{\rm CN}(\epsilon)$ and $\sigma_{\rm FF}(\epsilon)$ were computed from empirical expressions [15] which are a good representation of those of Becchetti and Greenlees for

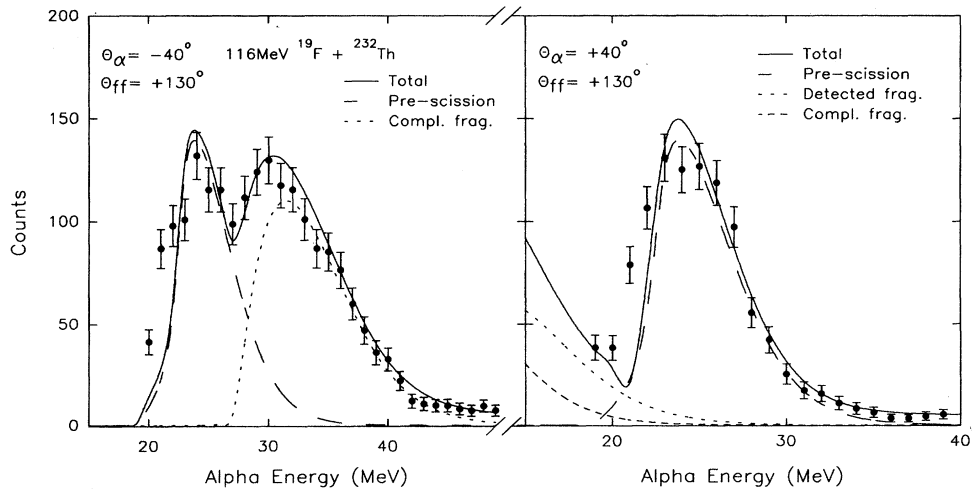

FIG. 2. The same as Fig. 1, for alphas.

TABLE I. Measured prescission multiplicities (π_{pre}, α_{pre}), postscission multiplicities (π_{post}, α_{post}), and mean center-of-mass kinetic energies (ϵ_π, ϵ_α) of prescission particles for $^{19}F + ^{232}Th$.

E_{lab} (MeV)	E_x (MeV)	π_{pre} (10^{-3})	π_{post} (10^{-3})	ϵ_π (MeV)	α_{pre} (10^{-3})	α_{post} (10^{-3})	ϵ_α (MeV)
104	55.5	2.7±0.4	2.8±0.4	11.7±0.5	2.1±0.2	2.4±0.2	21.2±0.5
110	61.1	3.3±0.5	2.4±0.4	11.5±0.5	2.7±0.3	2.7±0.3	21.4±0.5
116	66.7	5.1±0.7	2.2±0.3	12.0±0.5	4.2±0.4	2.6±0.3	21.6±0.5
118	68.5	6.2±0.7	2.2±0.2	11.8±0.5	7.4±0.4	2.7±0.2	21.0±0.5

protons [16] and Huizenga and Igo [17] for α particles. In order to fit the experimental spectra, it was necessary to reduce the Coulomb barriers for proton and α emission from the compound nucleus. Barrier shifts of 1.5 MeV for protons and 2.0 MeV for α particles resulted in a good fit to the data at all the energies and were not varied for the individual fits. The multiplicities were obtained by integrating the fitted spectra. The fits to the prescission proton and alpha spectra at 116 MeV are shown in Figs. 1 and 2 and similar fits were obtained at the other energies.

Our analysis includes a small correction for the effect of anisotropy of the emitted particles with respect to the spin direction of the compound system [7].

The extracted pre- and postscission multiplicities and the mean center-of-mass kinetic energies of the prescission particles are given in Table I. Figure 3 shows the prescission proton and alpha multiplicities of the present measurement as a function of beam energy, along with the prescission neutron data from an earlier measurement [2].

IV. STATISTICAL MODEL ANALYSIS

The prescission data have been analyzed using the statistical model in order to extract the prescission time scales. Calculations without incorporating fission delay or Coulomb barrier shifts and with a level density parameter of $a=A/10$ MeV^{-1} using the code PACE2 [18] are shown as dashed curves in Fig. 3. These calculations underpredict the data by about a factor of 10.

In Ref. [7], it is shown that the effects of deformation on the particle binding energies as well as on the particle transmission coefficients are important and the time scales extracted from charged particle data are not consistent with those obtained from neutron data without incorporating these effects. We have used the code JOANNE2 where these effects are included. The deformation-dependent level densities of Toke and Swiatecki [19] have been used in these calculations. Prescission emission is assumed to take place from two points in the deformation space, corresponding to presaddle and saddle-to-scission emission. The time scales for these two processes (t_d and t_{ssc}) and the mean deformation of the saddle-to-scission emitter (Z_{axis}), have been varied to reproduce the data.

The emission of prescission particles at a given deformation Z_0, depends upon the deformation energy, the particle binding energies, and the transmission coefficients. The deformation energies for $^{19}F+^{232}Th$ as a function of Z_0, are shown in Fig. 4. These calculations were made using the deformed liquid drop model code DEFMASS [20]. The charged particle binding energies (Fig. 5) and transmission coefficients (Fig. 6) vary strongly with deformation. For neutrons the binding energy does not vary substantially with deformation. While the multiplicities ν_{pre}, π_{pre}, and α_{pre} were found to be sensitive to t_d, t_{ssc}, and Z_{axis}, the mean emission energies of the charged particles were relatively insensitive.

The compound nucleus angular momentum distributions were calculated using the code CCDEF [21] with parameters adjusted to fit the measured fission excitation function [22]. Charged particle multiplicities, especially α particle multiplicities, are sensitive to the angular momentum distribution,

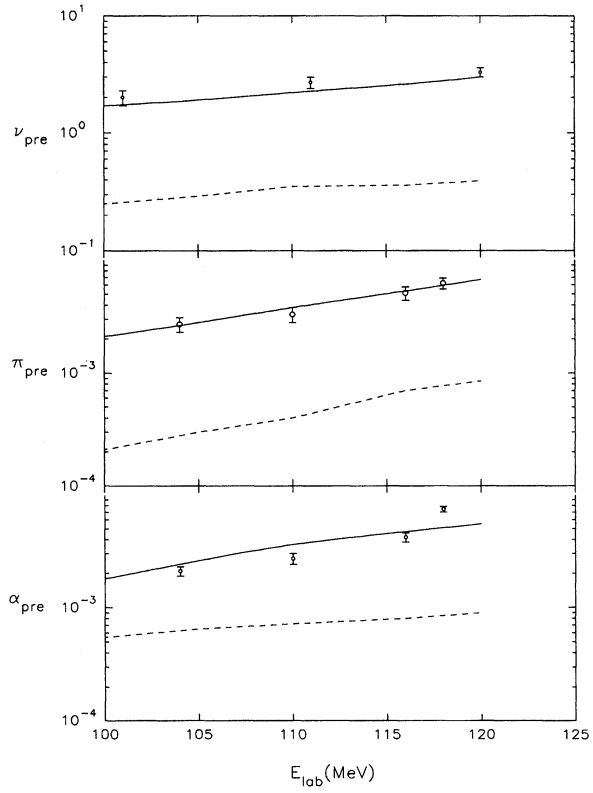

FIG. 3. The measured prescission proton and α multiplicities. The prescission neutron multiplicities are from Ref. [2]. The dashed lines are calculations using the code PACE2 with spherical nucleus Coulomb barriers $a=A/10$ MeV^{-1} and without fission delay. The solid curves are calculations using the code JOANNE2 with $t_d=20$ zs, $t_{ssc}=20$ zs and deformation-dependent particle binding energies, transmission coefficients, and level densities.

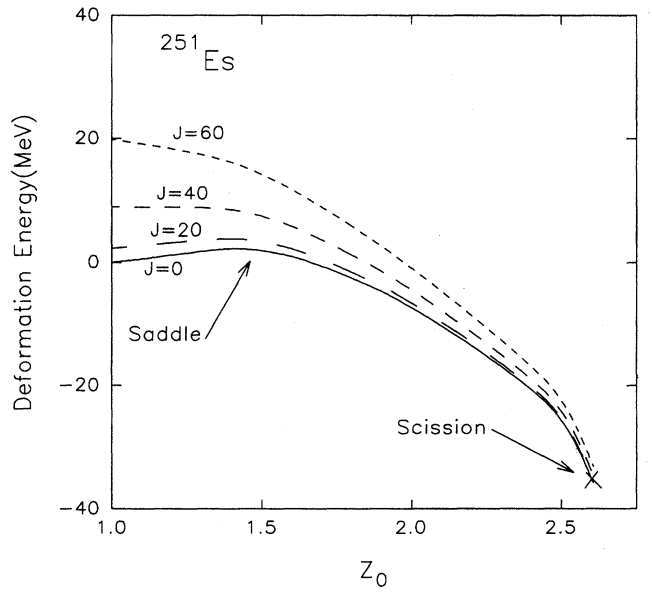

FIG. 4. The potential energy diagram for ^{251}Es showing the deformation energy as a function of deformation for angular momentum, $J=0$, $20\hbar$, $40\hbar$ and $60\hbar$.

the multiplicities being enhanced for larger l values.

The calculations using the code JOANNE2 were made varying t_d, t_{ssc} for fixed values of Z_{axis} to separately fit the ν_{pre}, π_{pre}, and α_{pre} data. The results of the calculation with $Z_{axis}=2.22$, which corresponds to a point about halfway between saddle and scission, are shown in Fig. 7. In this figure, the correlated curves of t_{ssc} against t_d which give a fit to the prescission neutron, proton, and alpha multiplicities are plotted. The curves are well separated form each other, indicating that different fission lifetimes are required for understanding the ν_{pre}, π_{pre}, and α_{pre} data. The proton data require a total time scale in the range of $t_{fiss}=80$–110 zs, the neutron data, 40–80 zs, and the α data, 20–55 zs.

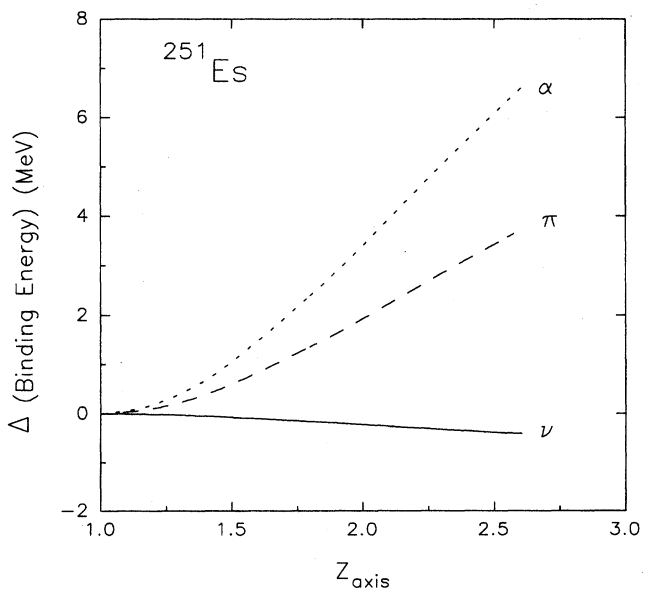

FIG. 5. Deformed liquid drop model predictictions of the deviation of binding energies from those for a spherical nucleus for neutron, proton, and α emission.

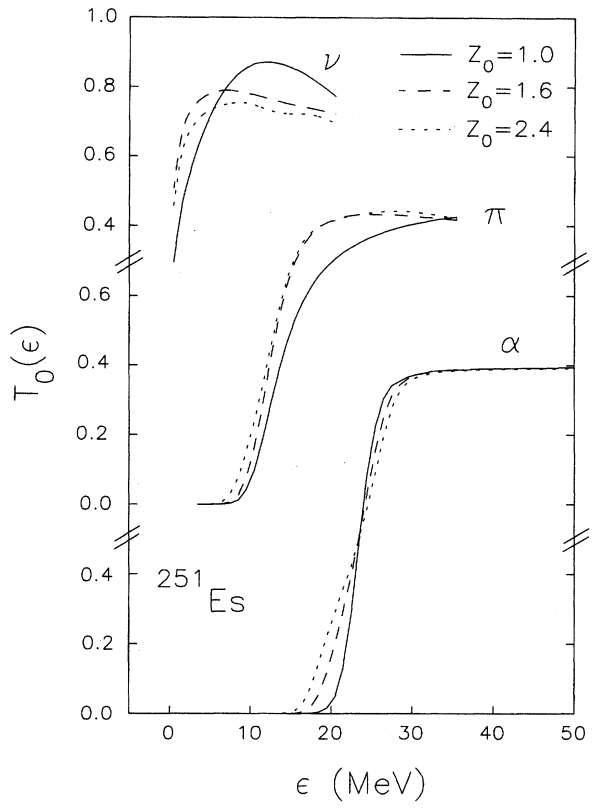

FIG. 6. Deformed liquid drop model predictictions of the $l=0$ transmission coefficients as a function of emission energy for neutrons, protons, and α particles.

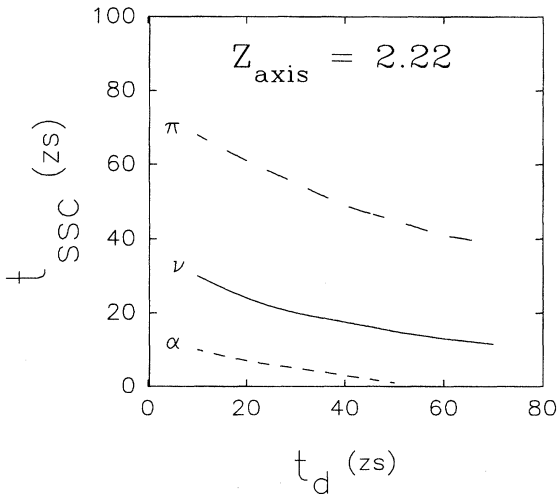

FIG. 7. Correlated curves of the time scales t_{ssc} against t_d which result in fits to the prescission neutron, proton, and α multiplicities for an average deformation of the saddle-to-scission emitter, $Z_{axis}=2.22$.

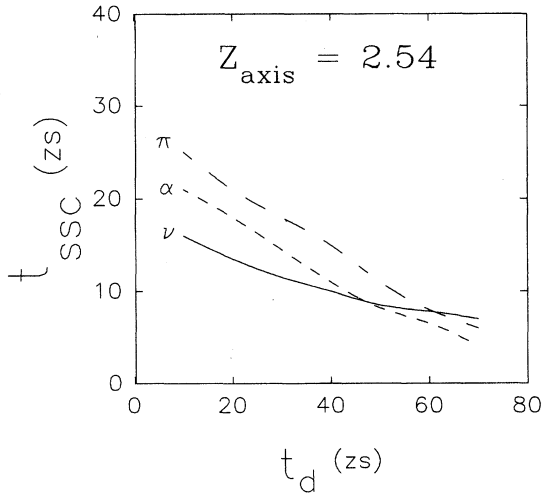

FIG. 8. The same as Fig. 7, for $Z_{axis}=2.54$.

However, the results are quite sensitive to Z_{axis}. Figure 8 shows a similar calculation for Z_{axis} fixed at 2.54, which corresponds to a deformation close to the scission point. In this case the three curves are closer together, implying consistent values of t_d, t_{ssc} from the neutron, proton, and α data. This figure shows that the best fit to the neutron, proton, and alpha prescission data arises with $Z_{axis}=2.54$, $t_d=50$ zs, $t_{ssc}=10$ zs. However, considering experimental errors, other combinations of t_d, t_{ssc} also result in a satisfactory description of the data. Thus, the individual time scales t_d and t_{ssc} could not be determined in the analysis. However, the total fission time-scale t_{fiss} is inferred to be in the range of 25-80 zs. The analysis is sensitive to Z_{axis} and indicates that postsaddle emission takes place close to the scission point. The calculated prescission multiplicities with $t_d=20$ zs, $t_{ssc}=20$ zs (solid curves) are compared with the data in Fig. 3.

V. DISCUSSION AND CONCLUSIONS

The present measurements of prescission charged particle multiplicities along with existing neutron multiplicity data for $^{19}F + ^{232}Th$ can be consistently understood by including the effect of deformation on particle binding energies and transmission coefficients. The prescission multiplicities are sensitive to the mean deformation of the saddle-to-scission emitter, Z_{axis}. The deduced value of Z_{axis} corresponds to a point close to scission. For the ^{251}Es compound system, a system with large fissility, postsaddle emission is seen to occur closer to the scission point as compared to the ^{200}Pb system [7] where the corresponding point was about halfway between saddle and scission. The total fission time scale for ^{251}Es is deduced to be in the range of 25–80 zs.

The mean emission kinetic energies depend upon the binding energies, transmission coefficients, and the potential energy surface. The potential energy surface is slowly varying in the present case as compared to the ^{200}Pb system [7], and it was found that the emission energies are insensitive to the individual delays t_d, t_{ssc}.

The present analysis is based upon a simple model wherein prescission emission is assumed to take place at two fixed points in the deformation space, whereas a more realistic model would allow for particle emission continuously along the fission path. Such calculations using the Langevin model for fission [10] are necessary for a more complete understanding of the dynamics.

ACKNOWLEDGMENTS

We thank Dr. J.P. Lestone for making available the code JOANNE2 and useful correspondence. We also thank S.S. Kerekatte, A. Nijasure, and B.V. John for their help during the experiment and the Pelletron crew for smooth operation of the accelerator.

[1] D.J. Hinde, R.J. Charity, G.S. Foote, J.R. Leigh, J.O. Newton, S. Ogaza, and A. Chatterjee, Nucl. Phys. **A452**, 550 (1986); J.O. Newton, D.J. Hinde, R.J. Charity, J.R. Leigh, J.J.M. Bockhorst, A. Chatterjee, G.S. Foote, and S. Ogaza, *ibid.* **A483**, 126 (1988); W.P. Zank, D. Hilscher, G. Ingold, U. Jahnke, M. Lehmann, and H. Rossner, Phys. Rev. C **33**, 519 (1986); A. Gavron, A. Gayer, J. Boissevain, H.C. Britt, T.C. Awes, J.R. Beene, B. Cheynis, D. Drain, R.L. Ferguson, F.E. Obenshain, F. Plasil, G.R. Young, G.A. Petitt, and C. Butler, *ibid.* C **35**, 579 (1987); H. Rossner, D. Hilscher, D.J. Hinde, B. Gebauer, M. Lehmann, M. Wilpert, and E. Mordhorst, *ibid.* C **40**, 2629 (1989); D.J. Hinde, D. Hilscher, and H. Rossner, Nucl. Phys. **A502**, 497c (1989).

[2] D.J. Hinde, R.J. Charity, G.S. Foote, J.R. Leigh, S. Ogaza, and A. Chatterjee, Phys. Rev. Lett. **52**, 986 (1984); **53**, 2275(E) (1984).

[3] D.J. Hinde, D. Hilscher, and H. Rossner, Nucl. Phys. **A538**, 243c (1992); D.J. Hinde, *ibid.* **A553**, 255c (1993).

[4] A. Saxena, A. Chatterjee, R.K. Choudhury, S.S. Kapoor, and D.M. Nadkarni, Phys. Rev. C **49**, 932 (1994).

[5] H. Ikezoe, N. Shikazono, Y. Nagame, Y. Sugiyama, Y. Tomita, K. Ideno, I. Nishinaka, B.J. Qi, H.J. Kim, A. Iwamoto, and T. Ohtsuki, Phys. Rev. C **46**, 1922 (1992).

[6] J.P. Lestone, J.R. Leigh, J.O. Newton, D.J. Hinde, J.X. Wei, J.X. Chen, S.E. Elfstrom, and D.G. Popescu, Phys. Rev. Lett. **67**, 1078 (1991).

[7] J.P. Lestone, Phys. Rev. Lett. **70**, 2245 (1993); J.P. Lestone, J.R. Leigh, J.O. Newton, D.J. Hinde, J.X. Wei, J.X. Chen, S.E. Elfstrom, and M. Zielinska-Pfabe, Nucl. Phys. **A559**, 277 (1993).

[8] H. Ikezoe, Y. Nagame, I. Nishinaka, Y. Sugiyama, Y. Tomita, K. Ideno, S. Hamada, N. Shikazono, A. Iwamoto, and T. Ohtsuki, Phys. Rev. C **49**, 968 (1994).

[9] M. Thoennessen, D.R. Chakrabarty, M.G. Herman, R. Butsch, and P. Paul, Phys. Rev. Lett. **59**, 2860 (1987); R. Butsch, M. Thoennessen, D.R. Chakrabarty, M.G. Herman, and P. Paul, Phys. Rev. C **41**, 1530 (1990); M. Thoennessen, J.R. Beene, F.E. Bertrand, C. Baktash, M.L. Halbert, D.J. Horen, D.G. Sa-

rantities, W. Spang, and D.W. Scracener, Phys. Rev. Lett. **70**, 4055 (1993).

[10] P. Frobrich and I.I. Gontchar, Nucl. Phys. **A563**, 326 (1993); P. Frobrich, I.I. Gontchar, and N.D. Malitov, *ibid.* **A556**, 281 (1993); I.I. Gontchar and P. Frobrich, *ibid.* **A551**, 495 (1993).

[11] D.C. Biswas, V.S. Ambekar, L.M. Pant, B.V. Dinesh, and R.K. Choudhury, Nucl. Instrum. Methods A **340**, 551 (1994).

[12] P.A. DeYoung, R.L. McGrath, and W.F. Piel, Jr., Nucl. Instrum. Methods **226**, 555 (1984).

[13] P. Heeg, K.F. Hoffmann, M. Mutterer, J.P. Theobald, K. Weingärtner, J. Pannicke, F. Gönnenwein, G. Barreau, and B. Leroux, Nucl. Phys. **A409**, 379c (1983); M. Sowinski, M. Lewitowicz, R. Kupczak, A. Jankowski, N.K. Skobelev, and S. Chojnacki, Z. Phys. A **324**, 87 (1986).

[14] V.E. Viola, K. Kwiatkowski, and M. Walker, Phys. Rev. C **31**, 1550 (1985).

[15] A. Chatterjee, K.H.N. Murthy, and S.K. Gupta, Pramana J. Phys. **16**, 391 (1981).

[16] F.D. Becchetti and G.W. Greenlees, Phys. Rev. **182**, 1190 (1969).

[17] J.R. Huizenga and G. Igo, Nucl. Phys. **29**, 462 (1962).

[18] A. Gavron, Phys. Rev. C **21**, 230 (1980).

[19] J. Tōke and W.J. Swiatecki, Nucl. Phys. **A372**, 141 (1981).

[20] J.P. Lestone (private communication).

[21] J. Fernandez-Niello, C.H. Dasso, and S. Landowne, Comput. Phys. Commun. **54**, 409 (1989).

[22] S. Kailas, A. Navin, A. Chatterjee, P. Singh, A. Saxena, D.M. Nadkarni, D.C. Biswas, R.K. Choudhury, and S.S. Kapoor, Pramana J. Phys. **41**, 339 (1993).